ELSEVIER

Chemical Geology 238 (2007) 94–106

CHEMICAL GEOLOGY
INCLUDING
ISOTOPE GEOSCIENCE

www.elsevier.com/locate/chemgeo

Sorption of Ni by birnessite: Equilibrium controls on Ni in seawater

Caroline L. Peacock, David M. Sherman *

University of Bristol, Department of Earth Sciences, Bristol BS8 1RJ, UK

Received 4 July 2006; received in revised form 23 October 2006; accepted 28 October 2006

Editor: D. Rickard

Abstract

Synthetic hexagonal birnessite (Hx-birnessite) is a close analogue to natural poorly crystalline phyllomanganate phases found in soils and marine ferromanganese deposits. These phases are often highly enriched in trace metals such as Ni and Co. We measured the sorption of Ni(II) onto synthetic hexagonal birnessite (Hx-birnessite) from pH 1 to 7. EXAFS spectra show that, at pH 3.7, Ni is adsorbed to the Hx-birnessite surface above vacancy sites on {001} as a tridentate corner-sharing complex. We developed a surface complexation model for Ni adsorption based on the equilibria

$$3(\equiv Mn_2O^{-2/3}) + Ni^{+2} = (\equiv Mn_2O)_3Ni^0$$

$$3(\equiv Mn_2O^{-2/3}) + Ni^{+2} + H_2O = (\equiv Mn_2O)_3Ni(OH)^- + H^+$$

Using this surface complexation model, we predict the concentration of Ni in seawater in equilibrium with Ni-bearing birnessite found in hydrogenetic FeMn crusts and nodules. Our predicted results are in good agreement with observed Ni concentrations in seawater and suggest that the concentration of dissolved Ni in seawater is buffered by sorption to birnessite or a related MnO_2 phase. However, in addition to the surface complex, Ni also sorbs by structural incorporation into the vacancy site. In our synthetic samples at pH 7, EXAFS shows ~10% of Ni is structurally incorporated into Hx-birnessite. In natural birnessites found in marine ferromanganese crusts and nodules, EXAFS shows that all of the sorbed Ni is structurally incorporated. Structural incorporation suggests that Ni sorption may be irreversible.

Keywords: Nickel; Hexagonal birnessite; Adsorption; EXAFS spectroscopy; Surface complexation modelling

1. Introduction

The aqueous geochemistry of Ni can be strongly controlled by sorption onto Mn(III, IV) oxides (such as birnessite and δ-MnO_2) and Fe (hydr)oxides (such as goethite, α-FeOOH). Sorption of Ni(II) to Mn oxides controls the release of Ni during pyrite oxidation (Larsen and Postma, 1997) while sorption to Fe (hydr) oxides retards its mobility during the chemical weathering of ore deposits and leads to secondary Ni enrichment (e.g., Som and Joshi, 2002). In the marine environment, Ni is enriched on the order 10^6 in deep-sea FeMn nodules (Arrhenius, 1963) relative to its average seawater concentration. Trace metal species appear to show a preference for sorption onto Fe- or Mn-rich phases in FeMn deposits; Ni–Mn spatial and compositional correlations have been found in both FeMn

* Corresponding author.
E-mail address: dave.sherman@bris.ac.uk (D.M. Sherman).

0009-2541/$ - see front matter © 2006 Elsevier B.V. All rights reserved.
doi:10.1016/j.chemgeo.2006.10.019

nodules and crusts (e.g., Kumar et al., 1994; Dutta et al., 2001).

Natural and synthetic birnessites can have a triclinic or hexagonal structure (Drits et al., 1997). However, "birnessite" was originally assigned to a natural mineral showing hexagonal sheet symmetry (cf. Jones and Milne, 1956) and hexagonal symmetry has been found in common among most natural birnessites (cf. Jones and Milne, 1956; McKenzie, 1989; Post, 1992) and synthetic δ-MnO_2 (Villalobos et al., 2003). In fact, δ-MnO_2 is not a separate mineral to hexagonal birnessite: δ-MnO_2 simply has fewer stacks of phyllomanganate sheets (Manceau, personal communication, 2005). In triclinic birnessite (Tc-birnessite), all octahedral layer positions are filled with Mn(IV) and Mn(III) cations (Drits et al., 1997) and negative charge generated within the octahedral layers is balanced exclusively by hydrated interlayer cations (Villalobos et al., 2003). In hexagonal birnessite (Hx-birnessite), however, negative layer charge arises from Mn(III)-octahedra vacancies (Fig. 1a) and Mn(III) for Mn(IV) substitutions and is compensated by a combination of protons and interlayer cations, depending on pH (Drits et al., 1997). The differences in structural composition between Tc-birnessites and Hx-birnessites will affect their reactivity and mechanism of metal uptake. Hx-birnessites, for example, are reported to sorb metals above/below vacancy sites (Fig. 1b) present in the octahedral sheets (e.g., Appelo and Postma, 1999; Manceau et al., 2002a). Tc-birnessites do not possess vacancy sites (Drits et al., 1997) and are therefore unable to sorb metals by this mechanism. If hexagonal symmetry is indeed in common among most natural birnessites (cf. Jones and Milne, 1956; McKenzie, 1989; Post, 1992), then synthetic sorption experiments must use Hx-birnessite (or δ-MnO_2) to accurately represent natural systems.

Before we can model the fate and transport of Ni(II) in low temperature ore deposits and in groundwater, we need to know the mechanisms and equilibria involved in sorption of Ni(II) onto Mn(III,IV) (hydr)oxide surfaces. Sorption edges and isotherms for Ni(II) on MnO_2 (Murray, 1975; Gray and Malati, 1979; McKenzie, 1980; Green-Pedersen et al., 1997) have been measured; however, fitting the sorption edges to a surface complexation model is difficult without molecular information about the identity of the surface complexes. Murray (1975) reported a protons released to metal adsorbed ratio of close to 1 for Ni^{+2} adsorbed on hydrous MnO_2 indicating the formation of monodentate surface complexes; only one type of surface sorption site was required to explain the available data. Green-Pedersen et al. (1997) described adsorption of Ni^{+2} on

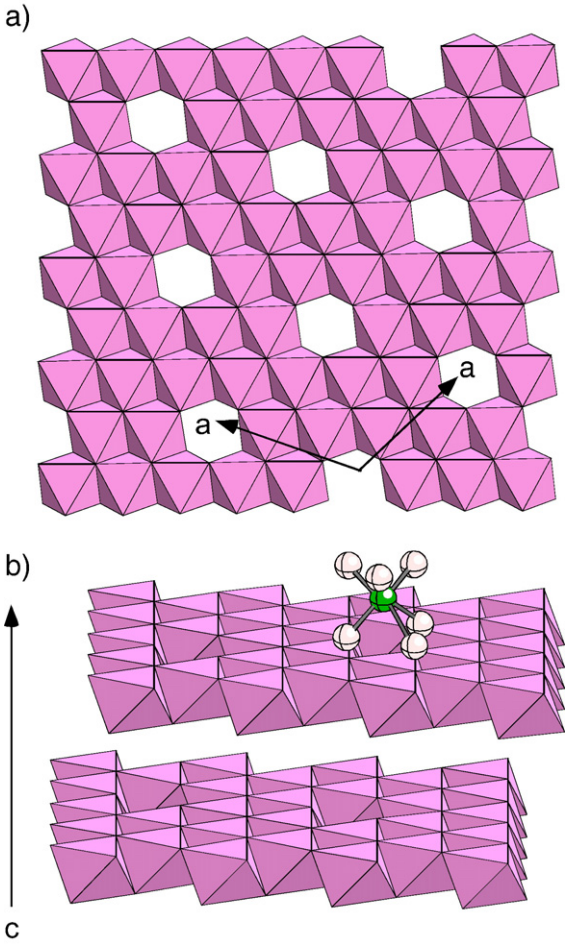

Fig. 1. (a) Structural model showing ordered vacancies in the phyllomanganate layer of Hx-birnessite. (b) Proposed surface complex for cations sorbed to Hx-birnessite. Surface complexes form above and below vacancy sites.

amorphous MnO with a Langmuir isotherm. Two-site surface complexation models (with ≡XOH and ≡YOH surface sites) have been invoked by Pretorius and Linder (2001) and Tonkin et al. (2004) to simulate divalent cation adsorption on δ-MnO_2 and model existing experimental data in the literature. Tonkin et al. (2004) successfully modelled the experimental data of Murray (1975) with the formation of $\equiv XONi^{+}$ and $\equiv XONiOH^{0}$ surface adsorption complexes. However, XAS data to date show most divalent cations adsorb to iron and manganese (hydr)oxides by forming bidentate and tridentate surface complexes, respectively (e.g., Peacock and Sherman, 2004a; Manceau et al., 2002a). It has been previously demonstrated that modelling alone cannot distinguish between otherwise plausible adsorption complexes (e.g., Westall and Hohl, 1980; Peacock and Sherman, 2004b), but to our knowledge there have been

no direct spectroscopic investigations of Ni(II) adsorption on Mn oxides. The crystal chemistry of Ni in some natural Mn oxides has, however, been investigated with XAS (e.g., Manceau et al., 1992, 2002b; Peacock and Sherman, in press).

To our knowledge, this is the first study to develop a surface complexation model of Ni(II) sorption to Hx-birnessite constrained by results from spectroscopy. Here, we fit sorption edges and isotherms to a surface complexation model based on surface species determined from EXAFS spectroscopy. Since the surface complexation models are based on actual surface species, we believe our results will be more reliable when applied to modelling uptake of Ni in complex natural systems.

2. Experimental methods

2.1. Mineral preparation and characterization

Synthetic Hx-birnessite was prepared by acidification of a triclinic Na-birnessite suspension (Drits et al., 1997; Silvester et al., 1997; Lanson et al., 2000; Liu et al., 2002). Triclinic Na-birnessite was prepared following the oxidation method of Liu et al. (2002). The product of the oxidation method is comparable to the triclinic Na-birnessite produced (on drying of Na-buserite) by following the redox method described by Giovanoli et al. (1970) and employed by Drits et al. (1997), Silvester et al. (1997) and Lanson et al. (2000).

Low crystalline Na-birnessite was obtained by pouring a mixed solution (100 ml) of 0.6 M NaOH and 3% H_2O_2 into a (50 ml) 0.3-M $Mn(NO_3)_2$ solution, while stirring vigorously at room temperature. The resulting precipitate was aged undisturbed in the reaction solution for 24 h. The precipitate was then filtered, washed with 18.2 MΩ MilliQ water and air-dried at room temperature. The drying precipitate was gently crushed to prevent the formation of large, hard particles. Higher crystalline Na-birnessite was then prepared by hydrothermal treatment of the low crystalline Na-birnessite in a 2-M NaOH solution at 175 °C for 15 h (Feng et al., 2000; Liu et al., 2002). The final precipitate was filtered, washed extensively with 18.2 mΩ MilliQ water and air-dried at room temperature. The drying precipitate was gently crushed to prevent the formation of large, hard particles. We used 18.2 mΩ MilliQ water and all reagents were AR grade.

Mineral identity and purity was confirmed by X-ray powder diffraction (XRD) analysis of randomly orientated powder samples before, after 5 h and after 15 h hydrothermal treatment. The XRD pattern of our synthetic Na-birnessite corresponds to the birnessite-type sodium manganese oxide with a basal spacing of 0.723 nm (see Liu et al., 2002). The five main lines identified by Liu et al. (2002) are present and correct at 7.23, 3.59, 2.52, 2.42 and 2.15 Å. Our sample closely matches the triclinic Na-birnessite produced by following the redox method (Drits et al., 1997; Silvester et al., 1997; Lanson et al., 2000, 2002; Villalobos et al., 2003) and synthetic Na-birnessite JCPDS 23-1046 where the eight most intense d-spacings (intensity ≥ 10%) are 7.09 (100), 3.56 (80), 2.51(70), 2.42(60), 2.21(40), 2.15(40), 1.47(60) and 1.43(50) Å.

Hx-birnessite was obtained by dispersing triclinic Na-birnessite in 0.1 M $NaNO_3$ (~2 g/L) and adjusting the pH to approximately pH 2 with 1 M HNO_3 (similar to the method of Silvester et al., 1997). The suspension was stirred for several hours at 25 °C. The resulting product was filtered, washed extensively with 18.2 MΩ MilliQ water and air-dried at room temperature. Mineral identity and purity were confirmed by XRD analysis of randomly orientated powder samples. The XRD pattern of our synthetic Hx-birnessite is shown in Fig. 2 and closely matches the hexagonal H^+-birnessite XRD pattern published by Drits et al. (1997). $d(100)/d(110) \approx \sqrt{3}$ confirms the synthesis of Hx-birnessite. The surface area of the final Hx-birnessite was measured by BET to be 35±3 m^2/g.

2.2. Potentiometric titration

Hx-birnessite potentiometric titrations were carried out at 0.1 M $NaNO_3$ salt concentration, following the generalized potentiometric titration method of Hayes et al. (1991). Titrations were performed at 25 °C in an air-tight reactor with constant stirring to prevent settling. Dried solid Hx-birnessite (0.1 g) was suspended in

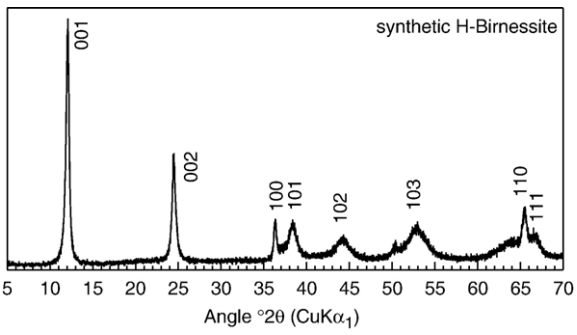

Fig. 2. X-ray diffraction pattern of synthetic Hx-birnessite showing 001, 002, 100 and 110 reflections corresponding to d-spacings of ~7 Å, ~3.6 Å, ~2.4 Å and ~1.4 Å, respectively.

50 mL of 0.1 M $NaNO_3$ prepared with pre-boiled, nitrogen purged (<1 ppm CO_2 (g)) 18.2 MΩ MilliQ water. The suspension was nitrogen-purged (<1 ppm CO_2 (g)) for several hours prior to titrations. Initial pH after several hours purging was ~pH 3. Base (0.01 M NaOH, free from carbonate, in 0.1 M $NaNO_3$) and acid (0.1 M HNO_3) were prepared from stock solutions and added via an automated titrator. The suspension was initially titrated with base to ~pH 10, then the suspension was returned to ~pH 2 by reverse acid titration. After each incremental addition of base or acid, up to 30 min were allowed for pH equilibration. Stabilization of pH to two decimal places was always achieved within 30 min. A nitrogen atmosphere (<1 ppm CO_2 (g)) was maintained throughout the experiment. No significant hysteresis was observed between the base and the acid leg.

We used a pin-tip double junction glass combination electrode (Sentek) with a salt bridge of 3 M $NaNO_3$. The electrode was calibrated potentiometrically following the method of Gans and O'Sullivan (2000).

The acid leg of the titrations is reported in Section 3.3 and used to optimize acid–base parameters for use in nickel–Hx-birnessite surface complexation modelling.

2.3. Sample synthesis

Hx-birnessite batch experiments were prepared with Ni(II) aqueous solution using AR grade reagents and 18.2 MΩ MilliQ water. All solutions and resulting experimental suspensions were purged with N_2 (g) (<1 ppm CO_2 (g)) and all adsorption experiments were conducted at 25 °C. pH measurements were calibrated to ±0.05 pH units using Whatman NBS grade buffers.

2.3.1. pH adsorption edge experiment

Ni(II) stock solution was prepared at 100 ppm from $Ni(NO_3)_2{\cdot}6H_2O$. Adsorption pH experiments at 60 ppm $[Ni]_{total}$ were prepared by adding 18.0 ml of 100 ppm Ni stock solution to 0.2 g Hx-birnessite in 12.0 ml of 0.1 M $NaNO_3$. Sorbent concentration in solution was therefore 6.67 g/L. The resulting suspensions were immediately shaken and initial pH was recorded after stabilization to two decimal places. Initial pH was always below that required for precipitation of Ni(OH) (s). Suspension pH was then varied from ~pH 1 to 7 by the dropwise addition (<1 ml) of HNO_3/NaOH and recorded after stabilization to two decimal places. At sorption edge points ~pH 7, addition of 60 ppm $[Ni]_{total}$ to the sorbent suspension was performed incrementally and pH was raised slowly to allow sorption of Ni onto Hx-birnessite rather than precipitation of Ni as $Ni(OH)_2$ (s) in solution. Adsorption pH experiments were then shaken continuously for 24 h. Adsorption of Ni to Hx-birnessite at 60 ppm $[Ni]_{total}$ was investigated with EXAFS spectroscopy of specific samples from the adsorption edge at pH 3.7 and 7. Hx-birnessite samples at pH 3.7 and 7 contained 0.87 and 0.90 wt.% Ni with estimated surface coverage (calculated from the optimized total active surface site density, Table 2) at ~11.3% and 11.6%, respectively.

2.3.2. Constant-pH isotherm experiments

Constant-pH isotherms were measured at pH 3.6 and 7 and prepared under N_2 (g) (<1 ppm CO_2 (g)).

Ni(II) stock solution was prepared at 1000 ppm from $Ni(NO_3)_2.6H_2O$. Constant-pH experiments were prepared by adding 0.09–4.95 ml of 1000 ppm Ni stock solution to 0.048 g Hx-birnessite in 44.91–40.05 ml of 0.1 M $NaNO_3$, respectively. Sorbent concentration in solution was therefore 1.067 g/L, and $[Ni]_{total}$ ranged from 2 to 110 ppm. The resulting suspensions were immediately shaken and initial pH was recorded after stabilization to two decimal places. Initial pH was always below that required for precipitation of $Ni(OH)_2$ (s) as calculated using PHREEQC (Parkhurst and Appelo, 1999). The aqueous speciation of Ni and the solubility of $Ni(OH)_2$ will be discussed below. Suspension pH was then adjusted to that of the experiment by the dropwise addition (<1 ml) of HNO_3/NaOH and recorded after stabilization to two decimal places. At constant-pH 7, addition of >90 ppm $[Ni]_{total}$ to the sorbent suspension was performed incrementally and pH was raised slowly to allow sorption of Ni onto Hx-birnessite rather than precipitation of Ni as $Ni(OH)_2$ (s) in solution. Constant-pH experiments were then shaken continuously for 24 h.

Batch adsorption samples were separated by centrifugation (10,000 rpm for 5–10 min) into an adsorption sample (thick paste) for spectroscopic analysis and a clear supernate for determination of total nickel concentration. Supernates were filtered using 0.2 μm cellulose nitrate membrane filters, acidified with 1% HNO_3 and analyzed for nickel by inductively coupled plasma atomic emission spectrometry (ICP-AES). Spectroscopy was performed after storage at 1–4 °C for a maximum of 24 h.

2.4. Surface complexation modelling

The program FITEQL v3.2 (Herbelin and Westall, 1996) was used to fit the acid–base behavior of the Hx-birnessite surfaces and subsequently the adsorption

behavior of Ni on Hx-birnessite to a surface complexation model. FITEQL is used extensively for the calculation of chemical equilibrium constants in metal adsorption studies (e.g., Tonkin et al., 2004). The quality of the fits produced is given by:

$$V(Y) = (Y/S)^2/(n_p{*}n_{II} - n_u). \quad (1)$$

where Y is the actual error in the mass balance equation, S_Y is the estimated experimental error given by FITEQL and the reciprocal of the variance S_Y is the weighting factor. n_p is the number of data points, n_{II} is the number of chemical components with known total and free concentrations and n_u is the number of adjustable parameters (Lumsdon and Evans, 1994; Gao and Mucci, 2001). A good fit to experimental metal binding data is indicated by a value of $V(Y)$ between 0.1 and 20 (Herbelin and Westall, 1996).

2.5. EXAFS data collection and analysis

2.5.1. Data collection

EXAFS fluorescence spectra of the Ni K edge (8333 eV) were collected on station 7.1 at the CLRC Synchrotron Radiation Source, Daresbury Laboratory, UK. Synthetic Hx-birnessite adsorption samples were presented to the X-ray beam as a wet paste held by Sellotape in a 2-mm-thick Teflon slide with a 4 × 15 mm sample slot. During data collection, storage ring energy was 2.0 GeV and the beam current varied between 130 and 240 mA. The monochromator was set to reject 30% of the incoming beam to minimize higher harmonics in the EXAFS spectrum. EXAFS data were collated from up to 30 fluorescence mode scans using an Ortec 18-element solid state detector.

2.5.2. Data analysis

EXAFS data reduction was performed using Daresbury Laboratory software (EXCALIB, and EXBACK; Dent and Mosselmans, 1992). EXCALIB was used to calibrate from monochromator position (millidegrees) to energy (eV) and to average multiple spectra from individual samples. EXBACK was used to define the start of the EXAFS oscillations (determined from the inflection point on the K edge) and perform background subtraction. The pre-edge was fit to a linear function and the post-edge background to two 2nd-order polynomial segments. EXAFS were fit in the small atom approximation and we allowed for multiple scattering as coded in EXCURV98 (Binsted, 1998). The three-dimensional coordination environment about the Ni atom was modelled using a cluster with C_3 symmetry (Fig. 3a). This allows for the full multiple scattering analysis with the smallest number of independent parameters. Lowering the symmetry to C_1 and treating each atom independently did not statistically improve the EXAFS fits. To model the EXAFS spectrum at pH 7, it was necessary to include the structural incorporation of Ni into Hx-birnessite in addition to surface adsorption of Ni above vacancy sites. This was done using a linear combination of two

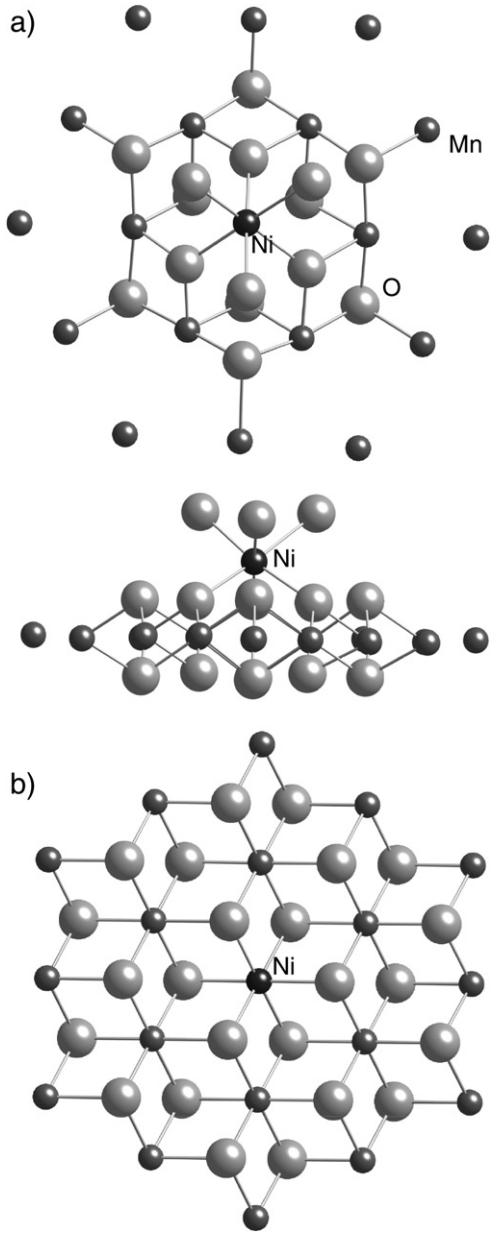

Fig. 3. Clusters used to model EXAFS spectra of (a) Ni(II) sorbed on synthetic Hx-birnessite (top and side view) and (b) Ni(II) incorporated into synthetic Hx-birnessite.

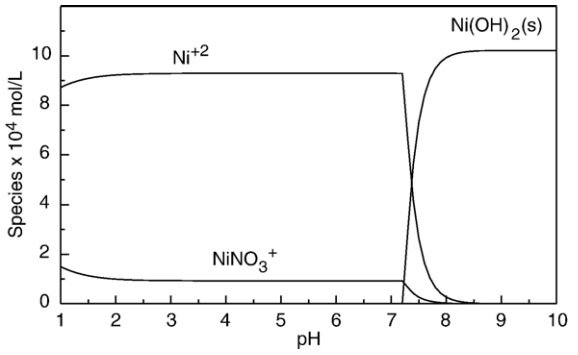

Fig. 4. Speciation of nickel(II) as a function of pH. $[Ni]_{total}=1.0\times10$ molal (~60 ppm) in 0.1 M $NaNO_3$ (calculated by suppressing the formation of NiO (s); hydrolysis stability constants from Baes and Mesmer, 1976).

clusters with C_3 symmetry (Fig. 3a for surface adsorption and Fig. 3b for structural incorporation). The phase–shift functions used in the curve fitting were derived by *ab initio* methods in EXCURV98 using Hedin–Lundqvist potentials (Hedin and Lundqvist, 1969) and von Barth ground states. No Fourier filtering was performed during the data analysis.

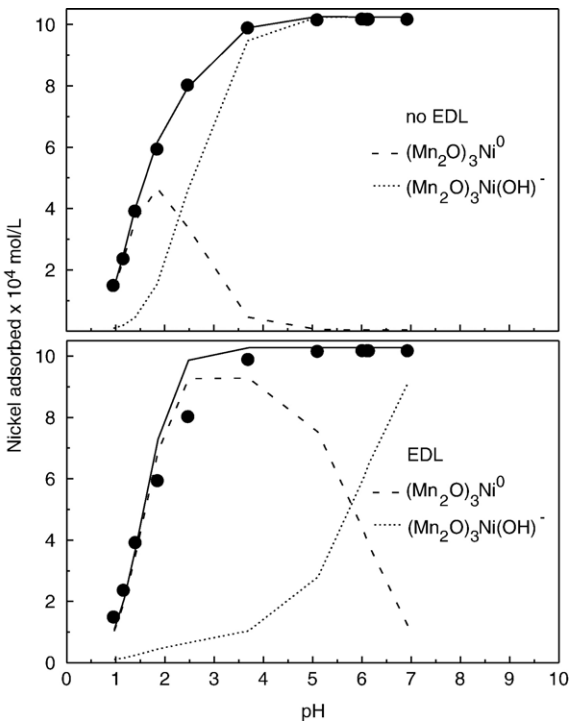

Fig. 5. Adsorption of nickel(II) ions to Hx-birnessite (6.67 g/L) as a function of pH at $I=0.1$ M $NaNO_3$ and 25 °C, after 24 h equilibration time with 60 ppm $[Ni]_{total}$. Symbols are data points; lines are model fits: no EDL indicates data were fit with the no EDL model; EDL indicates data were fit with the diffuse layer model (DLM).

3. Results and discussion

3.1. Aqueous speciation of Ni and sorption on Hx-birnessite

We measured the sorption of Ni(II) onto synthetic Hx-birnessite from ~pH 1 to 7 at 60 ppm $[Ni]_{total}$. The aqueous speciation of Ni^{+2} at 60 ppm $[Ni]_{total}$ in 0.1 M $NaNO_3$ and 25 °C (calculated using PHREEQC (Parkhurst and Appelo, 1999) and the stability constants in Table 3) is shown in Fig. 4 as a function of pH. In 0.1 M $NaNO_3$ between ~pH 1 and 7.2, Ni(II) occurs predominantly as the Ni^{+2} aqueous cation. Above ~pH 7.2, the formation of $Ni(OH)_2$ (s) begins to limit the concentration of aqueous Ni^{+2}. Above ~pH 7.4, Ni $(OH)_2$ (s) is the major form of Ni(II) present in the system. At 60 ppm $[Ni]_{total}$ and between ~pH 1 and 7, thermodynamic data (Table 3) predict that there is no Ni $(OH)_2$ precipitation and Ni(II) therefore likely sorbs as Ni^{+2} (aq) (Fig. 5).

We also measured the sorption of Ni(II) onto synthetic Hx-birnessite at constant-pH 3.6 and 7

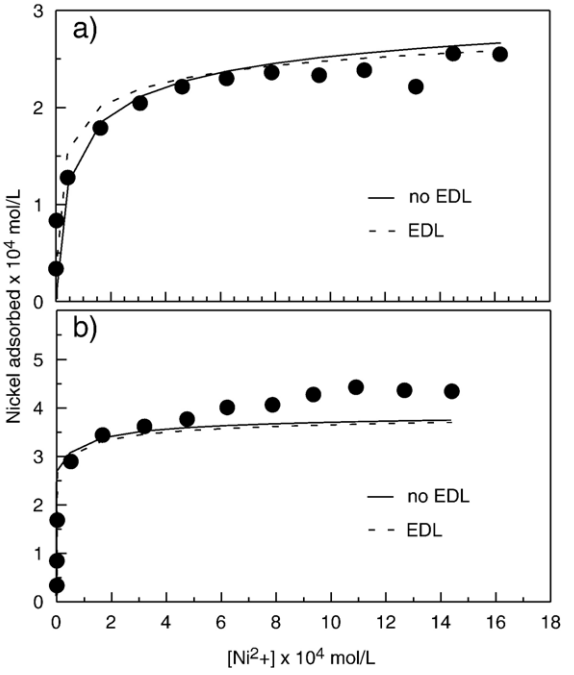

Fig. 6. (a) Adsorption of nickel(II) ions to Hx-birnessite (1.067 g/L) at constant-pH 3.6, $I=0.1$ M $NaNO_3$, and 25 °C, after 24 h equilibration time with 2–110 ppm $[Ni]_{total}$. (b) Adsorption of nickel(II) ions to Hx-birnessite (1.067 g/L) at constant-pH 7, $I=0.1$ M $NaNO_3$, and 25 °C, after 24 h equilibration time with 2–110 ppm $[Ni]_{total}$. Symbols are data points; lines are model fits: no EDL indicates data were fit with the no EDL model; EDL indicates data were fit with the diffuse layer model (DLM).

between 2 and 110 ppm $[Ni]_{total}$ (Fig. 6). At pH 3.6 and 7 in 0.1 M $NaNO_3$, thermodynamic data (Table 3) predict that Ni(II) occurs predominantly as the aqueous Ni^{+2} cation between $[Ni]_{total}$ 2 and 110 ppm; at pH 7.1, precipitation of $Ni(OH)_2$ (s) is predicted to occur at 110 ppm (1.874×10^{-3} mol/L) aqueous Ni(II). At constant-pH 7, addition of >90 ppm $[Ni]_{total}$ to the sorbent suspension was therefore performed incrementally and pH was raised slowly to allow sorption of Ni onto Hx-birnessite rather than precipitation of Ni as Ni $(OH)_2$ (s) in solution. Precipitation of $Ni(OH)_2$ (s) would be shown on Fig. 6 by a sharp increase in $[Ni^{+2}]$. At a constant-pH of both pH 3.6 and 7, Fig. 6 shows that there is no $Ni(OH)_2$ (s) precipitation and Ni(II) therefore likely sorbs as Ni^{+2} (aq).

3.2. EXAFS of Ni sorbed on Hx-birnessite

Ni *K* edge EXAFS (and Fourier transforms of the EXAFS) for Ni on synthetic Hx-birnessite sorbed at pH 3.7 and pH 7 are shown in Fig. 7 and summarized in Table 1. For the EXAFS spectra at pH 3.7, the coordination environment consists of 6 O at ~2.0± 0.05 Å and 6 Mn at ~3.5±0.05 Å. These distances are those expected for Ni sorption over vacancy sites on {001} (e.g., Appelo and Postma, 1999; Manceau et al., 2002a), where Ni is bonded to three surface oxygens (Fig. 1b). To confirm this interpretation, we set up a full three-dimensional model for the Ni coordination environment using the cluster shown in Fig. 3a. This allows for inclusion of full multiple scattering with the EXCURV98 code. We can account for all of the features in the EXAFS spectrum of the sample at pH 3.7 by refinement with this cluster constrained to C_3 symmetry (e.g., all of the coordination numbers are fixed and equivalent distances are constrained to be equal). The resulting Ni–O, Ni–Mn distances and Debye–Waller factors are given in Table 1. Note that the uncertainty in the interatomic distances, ΔR, is determined by the *k*-range of the EXAFS spectra: for $k=3$–12 $Å^{-1}$, ΔR will be 0.05 Å. The uncertainty in the Debye–Waller factor of a shell is more difficult to estimate but, for a fixed coordination number, is on the order of 10%.

The EXAFS spectrum at pH 7, however, shows evidence for a Ni–Mn scattering at 2.9±0.05 Å. This distance is close to the Mn–Mn distance in the MnO_2

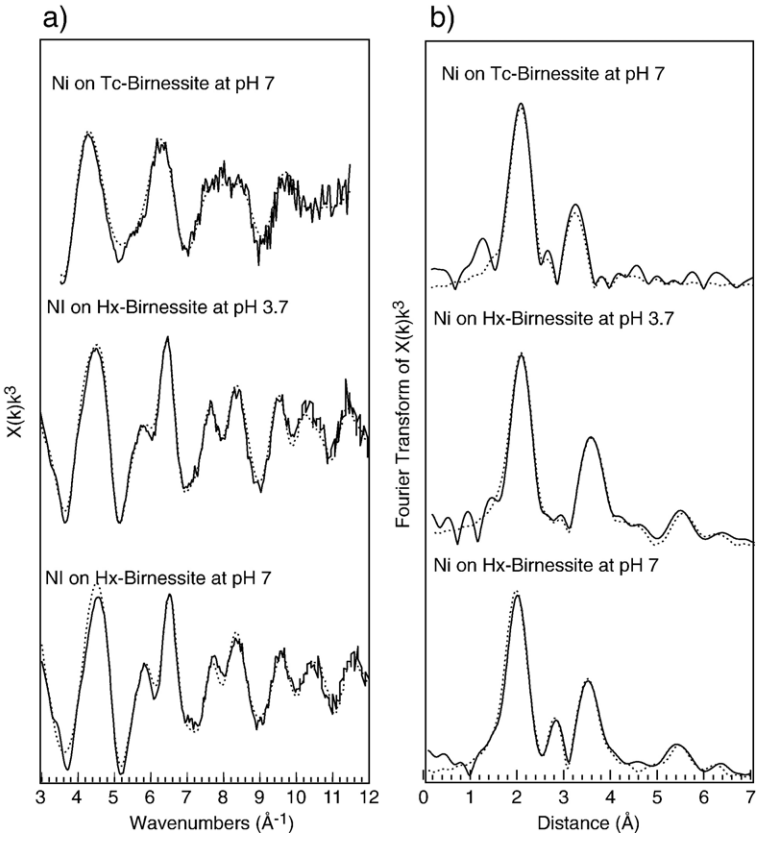

Fig. 7. (a) EXAFS and (b) Fourier transform of EXAFS for Ni(II) on synthetic Hx-birnessite adsorption samples equilibrated with 60 ppm $[Ni]_{total}$.

Table 1
EXAFS fits for Ni(II) on synthetic Hx-birnessite at pH 3.7 and 7

	N	R in Å	*θ*	*Φ*	$2\sigma^2$ in Å^2
Synthetic Hx-birnessite pH 3.7					
R=19%					
Ni_0	*1.0*	0.00	0.0	*0*	0.000
O_1	*3.0*	2.10	60.0	*270*	0.008
O_2	*3.0*	1.98	120.5	*90*	0.010
O_3	*3.0*	3.24	150.0	*270*	0.008
Mn_4	*3.0*	3.54	124.9	*0*	0.009
Mn_5	*3.0*	3.42	126.0	*180*	0.006
O_6	*3.0*	4.32	136.3	*90*	0.006
O_7	*3.0*	3.62	*110.0*	*270*	0.007
Mn_8	*3.0*	5.39	*110.0*	*90*	0.004
Mn_9	*3.0*	5.54	*110.0*	*270*	0.005
Mn_{10}	3.0	5.97	110.0	0	0.008
Mn_{11}	*3.0*	5.77	*110.0*	*180*	0.007
Synthetic Hx-birnessite at pH 7					
R=22%					
Ni_0	0.9	0.00	0.0	*0*	0.000
O_1	*3.0*	2.10	60.0	*270*	*0.010*
O_2	*3.0*	1.98	120.5	*90*	0.010
O_3	*3.0*	3.24	150.0	*270*	0.008
Mn_4	*3.0*	3.54	124.9	*0*	0.009
Mn_5	*3.0*	3.42	126.0	*180*	0.006
O_6	*3.0*	4.32	136.3	*90*	0.006
O_7	*3.0*	3.62	*110.0*	*270*	0.007
Mn_8	*3.0*	5.39	*110.0*	*90*	0.004
Mn_9	*3.0*	5.54	*110.0*	*270*	0.005
Mn_{10}	*3.0*	5.97	*110.0*	*0*	0.008
Mn_{11}	*3.0*	5.77	*110.0*	*180*	0.007
Ni_{12}	0.1	0.00	0.0	*0*	0.000
O_{13}	*3.0*	2.06	47.0	*0*	0.010
O_{14}	*3.0*	2.00	135.6	*180*	0.007
Mn_{15}	*3.0*	2.83	*90.0*	*30*	0.010
Mn_{16}	*3.0*	2.88	*90.0*	*330*	0.008
Mn_{17}	*3.0*	5.92	*90.0*	*30*	0.007
Mn_{18}	*3.0*	4.93	*90.0*	*180*	0.007
Mn_{19}	*3.0*	5.04	*90.0*	*0*	0.007
Mn_{20}	*3.0*	5.91	*90.0*	330	0.008
O_{21}	*3.0*	3.35	105.0	*0*	0.007
O_{22}	*3.0*	3.50	75.0	*180*	0.008
O_{23}	*3.0*	4.55	75.6	*105*	0.007
O_{24}	*3.0*	4.52	105.0	*45*	0.007
O_{25}	*3.0*	4.52	100.0	*75*	0.008
O_{26}	*3.0*	4.47	75.0	*135*	0.007

N is the number of atoms in a shell. σ is the Debye–Waller factor. *R*, θ and Φ are the spherical coordinates of the prototype atom in each shell with C_3 symmetry. Values in italics were constrained. Uncertainties in *R* are ±0.05 Å.

layer and indicates that some of the sorbed Ni has been structurally incorporated by substitution for Mn^{3+}/Mn^{4+}. To model the EXAFS at pH 7, we used a linear combination of two clusters (Fig. 3a and b). The second cluster, corresponding to structural incorporation, was taken from the EXAFS fit of a natural Hx-birnessite that showed complete structural incorporation of Ni (Peacock and Sherman, in press). Except for the first two shells, the geometries of each cluster were held fixed so that only the relative Ni site occupancies were fit. This approach gave a statistically significant (>95%) improvement in the fit of the EXAFS and indicated that 10±2% of the Ni has been structurally incorporated. Since only a small fraction of Ni is incorporated and only at the highest pH, we believe that we can model the sorption edge (pH 1–7) in terms of surface complexes only.

The EXAFS of Ni sorbed to Hx-birnessite show no evidence for Ni sorbing to the edge-sites on the {001} surfaces defined by the edges of the MnO_2 layers. On triclinic birnessite (Tc-birnessite), however, there are no vacancy sites within the MnO_2 layers and only edge-site sorption is possible. Fig. 7 also shows the EXAFS of 0.9 wt.% Ni sorbed onto a Tc-birnessite. The first next-nearest neighbor shell consists of two Mn atoms at 3.05±0.05 Å, which is the distance expected for Ni sorbing to the edge sites via a tridentate corner-sharing complex. This feature would be resolvable in the spectra of Ni on Hx-birnessite.

3.3. Surface complexation modelling of Ni sorbed on Hx-birnessite

The layer structure of Hx-birnessite (space group $P6_3/mmc$) means that the dominant surface is the {001}. On the Hx-birnessite {001} surfaces, there are three doubly coordinated O_{II} oxygens associated with each vacancy site (Fig. 8). The edges of the phyllomanganate layers of Hx-birnessite are the {100} surfaces. On the

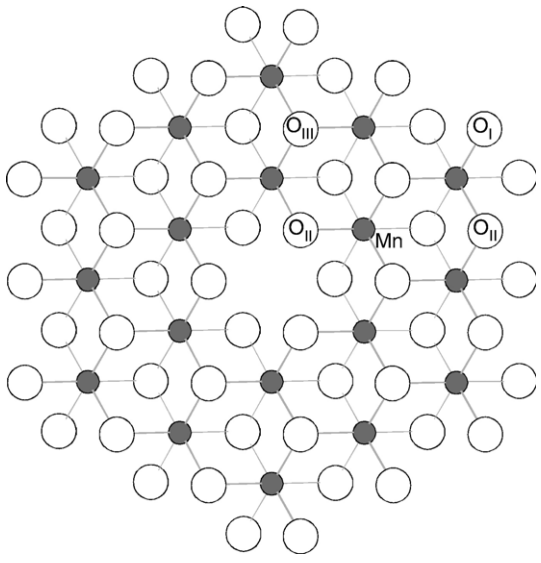

Fig. 8. Surface functional groups on Hx-birnessite.

{100} surfaces, there are two active functional groups: the doubly coordinated O_{II} oxygens and the singly coordinated O_I oxygens (Fig. 8). Using Pauling's second rule and assuming all Mn is +4, we model the O_I oxygens to be $-OH^{-1/3}$ and $-OH_2^{+2/3}$. The O_{II} oxygens are modelled as $-O^{-2/3}$ and $-OH^{+1/3}$. The triply coordinated oxygens on the {001} surfaces have a total Pauling bond strength of 2; consequently, we assume they are inert. Note that these charges are, at best, a crude approximation to relative charges of the actual surface oxygens. They are used only to provide an internally consistent set of point charges for use with the diffuse-layer (or other) model of changes in the surface electrostatic potential resulting from sorption/deprotonation. In light of our model for the surface oxygens, we fit the potentiometric titration of the surface with a 2-site 1 pK model

$$\equiv Mn_2O^{-2/3} + H^+ = \equiv Mn_2OH^{+1/3} \log K_1 \quad (2)$$

$$\equiv MnOH^{-1/3} + H^+ = \equiv MnOH_2^{+1/3} \log K_2 \quad (3)$$

K_1 refers to the protonation of the doubly coordinated O_{II} oxygens while K_2 refers to the protonation of the singly coordinated O_I oxygens (Fig. 8). An initial (minimum) guess for the total number of moles of surface sites was determined from the measured surface area and the crystallographic surface site density of O_I oxygens on the {100} surfaces with the initial constraint that the number of O_{II} oxygens is equal to that of the O_I oxygens.

Optimized values for K_1, K_2 and the total moles of surface O_I and O_{II} (per gram of Hx-birnessite) are listed in Table 2; the Hx-birnessite potentiometric titration data with model fit are shown in Fig. 9. The experimental pH_{PZC} (the pH where the surface charge is zero) for Hx-birnessite is ~pH 2.9; this value is similar to previously reported experimental values for birnessite group synthetic manganese oxides (e.g., 2.3 ± 0.2; Catts and Langmuir, 1986). The model fit of the acid–base data (Fig. 9) shows that a 2-site 1 pK diffuse layer model (DLM; Dzombak and Morel, 1990) produces a very good replication of the data. The concentration of surface O_I oxygens derived from the potentiometric titration data, when combined with the BET surface area measurement of 35 m^2/g yields a surface site density of ~5 O_I/nm^2. This value is consistent with the crystallographically determined O_I surface site density (~5 O_I/nm^2). The concentration of surface O_{II} oxygens derived from the potentiometric titration data, when combined with the BET surface area measurement of 35 m^2/g , yields a surface site density of ~17 O_{II}/nm^2; where surface O_{II} oxygens are present on both the {100} and {001} surfaces.

Table 2
Acid–base parameters used in Hx-birnessite–Ni surface complexation modelling

	Hx-birnessite
pH_{PZC} [a]	2.9
Surface area(m^2/g) [b]	35.0
[MnO] (mol/g) [c]	3.05×10^{-4}
[Mn_2O] (mol/g)	1.01×10^{-3}
log K_1^c	1.33
log K_2^c	4.31
$V(Y)$	1.26

[a] Determined from potentiometric titration data (this study).
[b] Determined from BET analysis (this study).
[c] Determined from FITEQL simulation of potentiometric titration data (this study).

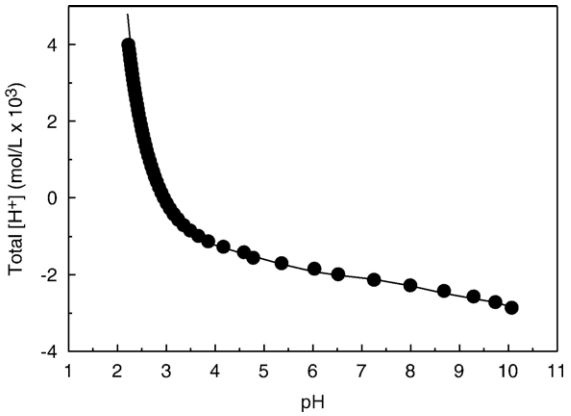

Fig. 9. Hx-birnessite potentiometric titration data at I=0.1 $NaNO_3$ and 25 °C, shown as total [H^+] in mol/L. 2 g/L oxide. Symbols are data points, line is DLM fit.

In light of our EXAFS results for Ni adsorbed on Hx-birnessite, we model our Ni/Hx-birnessite pH adsorption edge and constant-pH isotherm data using only the doubly coordinated surface O_{II} oxygens. Proposed surface complexes (Table 4) are able to occur at vacancy sites on {001}. These surface complexes are consistent with EXAFS indicating tridentate sorption. The number of moles of Mn_2O_{II} sites per gram of Hx-birnessite used in the modelling (Table 2) is therefore an upper limit as Mn_2O_{II} sites are present both on {001} and {100}. If we assume that the number of O_{II} oxygens is equal to that of the O_I oxygens on {100}, then the number of O_{II} oxygens on {001} can be approximated as $[O_{II}\ \text{oxygens}]_{total} - [O_I\ \text{oxygens}]_{\{100\}}$. Using the optimized total moles of surface O_I and O_{II} (Table 2), we calculate 7.05×10^{-4} mol $(Mn_2O_{II})_{\{001\}}$ sites per gram of Hx-birnessite. When repeating the surface complexation modelling (see below) using 7.05×10^{-4} mol $(Mn_2O_{II})_{\{001\}}$

Table 3
Ni complexes in experimental solutions

Species	Equilibrium expression	Log K	Ref.
$NiOH^+$	$Ni^{+2} + H_2O = NiOH^+ + H^+$	−9.86	1
$Ni(OH)_2^0$	$Ni^{+2} + 2H_2O = Ni(OH)_2^0 + 2H^+$	−19.00	1
$Ni(OH)_3^-$	$Ni^{+2} + 3H_2O = Ni(OH)_3^- + 3H^+$	−30.00	1
Ni_2OH^{+3}	$2Ni^{+2} + H_2O = Ni_2OH^{+3} + H^+$	−10.70	2
$Ni_4(OH)_4^{+4}$	$4Ni^{+2} + 4H_2O = Ni_4(OH)_4^{+4} + 4H^+$	−27.68	2
$NiNO_3^+$	$Ni^{+2} + NO_3^- = NiNO_3^+$	0.4	2
$Ni(OH)_2(s)$	$Ni^{+2} + 2H_2O = Ni(OH)_2 + 2H^+$	−10.8	1
H_2O	$2H_2O = OH^- + H^+$	−14.00	1

[1]Minteq database (Allison et al., 1990). [2]LLNL database (Wolery, 1979).

sites per gram of Hx-birnessite (rather than 1.01×10^{-3} mol $(Mn_2O_{II})_{total}$ sites per gram of Hx-birnessite (Table 2)), we find the fits to the Ni/Hx-birnessite pH adsorption edge and constant-pH isotherm data are the same (with log K's of the surface complexes increasing by ~0.5–1 log units).

Ni/Hx-birnessite pH adsorption edge and constant-pH isotherm data were modelled both by including the effect of the electrical double layer (using the DLM) and by completely neglecting any explicit representation of the surface electrostatics. The rational for this latter approach is that the surface electrostatics should only make a small contribution to the free energy of sorption if sorption occurs by the formation of strongly bound inner-sphere complexes. Thermodynamic data for reactions occurring in solution (Table 3), acid base parameters (Table 2) and surface complexes (Table 4) were used in both the model neglecting the electrical double layer (no-EDL) and the model including the electrical double layer (using the diffuse layer approximation).

The no-EDL and diffuse layer model fit to the Ni/Hx-birnessite pH adsorption edge data is shown on Fig. 5 and summarized in Table 4. Surface species (Table 4) were initially considered in a single-species framework for adsorption between pH 1 and 7. However, we find that the formation of $(\equiv Mn_2O)_3Ni^0$ and $(\equiv Mn_2O)_3Ni(OH)^-$ surface complexes (Table 4) provides the best fit to the observed Ni adsorption data. The formation of tridentate surface complexes is in agreement with our EXAFS data. We therefore fit the Hx-birnessite adsorption edge using the $(\equiv Mn_2O)_3Ni^0$ and $(\equiv Mn_2O)_3Ni(OH)^-$ surface complexes

$$3(\equiv Mn_2O^{-2/3}) + Ni^{+2} = (\equiv Mn_2O)_3Ni^0 \quad (4)$$

$$3(\equiv Mn_2O^{-2/3}) + Ni^{+2} + H_2O = (\equiv Mn_2O)_3Ni(OH)^- + H^+ \quad (5)$$

with stability constants

$$K_{Ni}\frac{\{(\equiv Mn_2O)_3Ni^0\}}{\{\equiv Mn_2O^{-2/3}\}^3[Ni^{+2}]\gamma_{Ni^{+2}}} \quad (6)$$

$$K_{NiOH} = \frac{\{(\equiv Mn_2O)_3Ni(OH)^-\}[H^+]\gamma_{H^+}}{\{\equiv Mn_2O^{-2/3}\}^3[Ni^{+2}]\gamma_{Ni^{+2}}}, \quad (7)$$

where square brackets indicate molalities and γ_{Ni} and γ_H are activity coefficients of aqueous ions calculated using the Davies equation. For a correct thermodynamic model, the surface species activities ({...}) should be given in terms of the mole fractions of surface sites and not in terms of the moles of sites/kg of water. We use as a standard state the hypothetical condition of complete coverage (over all vacancy sites) without being a surface precipitate.

From the potentiometric titration data, the total concentration of O_{II} oxygen surface sites was determined to be 1.01×10^{-3} mol/g (Table 2). From this, we fit the adsorption edge to give K_{Ni} (no-EDL)=2.40×10^3 (log K=3.38) and K_{NiOH} (no-EDL)=11.22 (log K=1.05). If we include the surface electrostatics using the Pauling-bond-strength-predicted charges and the diffuse layer model, we fit the sorption edge to give K_{Ni} (diffuse layer)=1.70×10^3 (log K=3.23) K_{Ni} (diffuse layer)=8.91 (log K=0.95) (Table 5). We tentatively recommend using K_{Ni} (no-EDL) and K_{NiOH} (no-EDL) for modelling Ni sorption over a pH range on Hx-birnessite with PHREEQC (version 2.0 and above) which uses the correct formalism for surface species

Table 4
Hx-birnessite–Ni surface complexation model reactions

Surface species	Equilibrium expression	Log K
$Mn_2O^{-2/3}$	$Mn_2O^{-2/3}$	
$Mn_2OH^{+1/3}$	$Mn_2O^{-2/3} + H^+ = Mn_2OH^{+1/3}$	1.33
$(\equiv Mn_2O)_3Ni^0$	$3(\equiv Mn_2O^{-2/3}) + Ni^{+2} = (\equiv Mn_2O)_3Ni^0$	K_{Ni}
$(\equiv Mn_2O)_3Ni(OH)^-$	$3(\equiv Mn_2O^{-2/3}) + Ni^{+2} + H_2O = (\equiv Mn_2O)_3Ni(OH)^- + H^+$	K_{NiOH}
$(\equiv Mn_2O)_3Ni(OH)_2^{-2}$	$3(\equiv Mn_2O^{-2/3}) + Ni^{+2} + 2H_2O = (\equiv Mn_2O)_3Ni(OH)_2^{-2} + 2H^+$	$K_{Ni(OH)2}$
$(\equiv Mn_2O)_3Ni(OH)_3^{-3}$	$3(\equiv Mn_2O^{-2/3}) + Ni^{+2} + 3H_2O = (\equiv Mn_2O)_3Ni(OH)_3^{-3} + 3H^+$	$K_{Ni(OH)3}$

Table 5
Predicted complexation of Ni^{+2} to synthetic Hx-birnessite

	no-EDL log K	Diffuse layer log K
K_{Ni}	3.38	3.23
K_{NiOH}	1.05	0.95
$V(Y)$	2.1	17.1

$K_{Ni}: 3(\equiv Mn_2O^{-2/3}) + Ni^{+2} = (\equiv Mn_2O)_3Ni^0$
$K_{NiOH}: 3(\equiv Mn_2O^{-2/3}) + Ni^{+2} + H_2O = (\equiv Mn_2O)_3Ni(OH)^- + H^+$

activities (Parkhurst and Appelo, 1999). Our fits of experimental data were checked with this code and the Minteq database (Allison et al., 1990).

The no-EDL and diffuse layer model fit to the Ni/Hx-birnessite constant-pH isotherm data at pH 3.6 and 7 is shown on Fig. 6. The pH adsorption edge data fit (Fig. 5) shows that, at both pH 3.6 and 7, the formation of $(\equiv Mn_2O)_3Ni(OH)^-$ surface complexes (Table 4) should be able to fit the observed Ni adsorption, and moreover, the formation of $(\equiv Mn_2O)_3Ni(OH)^-$ surface complexes should provide a better fit than the $(\equiv Mn_2O)_3Ni(OH)_2^{-2}$ and $(\equiv Mn_2O)_3Ni(OH)_3^{-3}$ complexes. Therefore in order to test our pH adsorption edge model, the constant-pH isotherm data at pH 3.6 and 7 was fit independently assuming no prior knowledge of best fit. This is important because the structure of Hx-birnessite changes with pH (e.g., Silvester et al., 1997). Again, surface species (Table 4) were initially considered in a single-species framework for adsorption between pH 1 and 7. In agreement with our pH adsorption edge modelling and our EXAFS for Ni adsorption onto synthetic Hx-birnessite, we find the constant-pH isotherm data at pH 3.6 and 7 is best fit by the formation of $(\equiv Mn_2O)_3Ni(OH)^-$ surface complexes in both a no-EDL and EDL (using the DLM) model. The fits are shown on Fig. 6. The goodness of fit parameter ($V(Y)$) is <20 for the no-EDL and diffuse layer model fit to the constant-pH 3.6 data, while a $V(Y)$ >20 for the no-EDL and diffuse layer model fit to the constant-pH 7 data likely reflects a slight under-estimation of the number of moles (Mn_2O_{II})total sites per gram of Hx-birnessite.

4. Application to ni in seawater

We can use our surface complexation model to predict the equilibrium concentration of dissolved Ni in equilibrium with Ni-bearing birnessite in hydrogenetic crusts and nodules. Such phases typically contain 4 wt. % Ni. In the model Hx-birnessite structure, 1/7 of the Mn sites are vacant. Hence, 4 wt.% Ni would correspond to a mole-fraction site occupancy of ~0.4. Using a model composition of seawater (Nordstrom et al., 1979), the Minteq database (Allison et al., 1990) of metal complex stability constants and total CO_3^{-2} of 0.1 mmol/kg, we predict that total dissolved Ni in seawater at pH 8.2 would be 7.2 nmol/kg. This is in close agreement with the mean Ni concentration of 2–12 nmol/kg (Bruland, 1983). Our calculation, however, is based on ion activity coefficients calculated using the Davies equation and is only approximate at the high ionic strength (0.6) of seawater. A further consideration is that at pH 7, we find some Ni has been structurally incorporated by substitution for Mn in the phyllomanganate layer and not as surface complexes above vacancies. Moreover, complete structural incorporation is found in natural phyllomanganate phases in marine ferromanganese crusts and nodules (Peacock and Sherman, in press). Whether structural incorporation over surface complexation has a strong effect on the solubility of Ni is unclear. Further molecular-level understanding of the energetics of Ni incorporation is needed.

Acknowledgments

Thanks are due to P. Chung Choi (University of Bristol) for assistance with ICP-AES. We also thank Chris Corrigan (Daresbury Materials Support Laboratory) for XRD and Fred Mosslemans (Daresbury Laboratory) for support at Station 7.1. We are especially grateful to Alain Manceau (University of Grenoble) for valuable discussion on the interpretation of Mn oxide XRD patterns. CLP was supported by a NERC studentship. Beamtime for EXAFS spectroscopy was provided by CLRC.

References

Allison, J.D., Brown, D.S., Novo-Gradac, K.J., 1990. MINTEQA2/PRODEFA2-A Geochemical Assessment Model for Environmental Systems—Version 3.0 User's Manual: Environmental Research Laboratory, Office of Research and Development. U.S. Environmental Protection Agency, Athens, Georgia. 106 pp.

Appelo, C.A.J., Postma, D., 1999. A consistent model for surface complexation on birnessite (−MnO_2) and its application to a column experiment. Geochim. Cosmochim. Acta 63, 3039–3048.

Arrhenius, G., 1963. Pelagic sediments. In: Hill, M.N. (Ed.), Sea, vol. 3. Interscience, New York, pp. 655–727.

Baes Jr, C.F., Mesmer, R.E., 1976. The hydrolysis of cations. John Wiley & Sons, New York.

Binsted, N., 1998. EXCURV98: The Manual. Daresbury Laboratory, Warrington, UK.

Bruland, K., 1983. Trace elements in seawater. In: Riley, J.P., Chester, R. (Eds.), Chemical Oceanography, vol. 8, 2nd edition. Academic Press, London, pp. 147–220.

Catts, J.G., Langmuir, D., 1986. Adsorption of Cu, Pb and Zn by δMnO_2: applicability of the site binding-surface complexation model. Appl. Geochem. 1, 255–264.

Dent, A.J., Mosselmans, J.F.W., 1992. A Guide to EXBACK, EXCALIB and EXCURV92. CLRC Daresbury Laboratory, Warrington, UK.

Drits, V.A., Silvester, E., Gorshkov, A.I., Manceau, A., 1997. Structure of synthetic monoclinic Na-rich birnessite and hexagonal birnessite: I. Results from X-ray diffraction and selected-area electron diffraction. Am. Mineral. 82, 946–961.

Dutta, R.K., Sideras-Haddad, E., Connell, S.H., 2001. Distribution of various components in a hydrogenous ferromanganese nodule and an Afanasiy Nikitin Seamount crust from Indian Ocean—a geochemical study using micro-PIXE. Nuc. Instrum. Methods Phys. Res., B 181, 545–550.

Dzombak, D., Morel, F.M.M., 1990. Surface Complexation Modelling Hydrous Ferric Oxide. John Wiley & Sons, New York, p. 10.

Feng, Q., Liu, L., Yanagisawa, K., 2000. Effects of synthesis parameters on the formation of birnessite-type manganese oxides. J. Mater. Sci. Lett. 19, 1567–1570.

Gans, P., O'Sullivan, B., 2000. GLEE: a new computer program for glass electrode evaluation. Talanta 51, 33–37.

Gao, Y., Mucci, A., 2001. Acid base reactions, phosphate and arsenate complexation, and their competitive adsorption at the surface of goethite in 0.7 M NaCl solution. Geochim. Cosmochim. Acta 65, 2361–2378.

Giovanoli, R., Stahli, E., Feitknecht, W., 1970. Uber oxidhydroxide des vierwertigen mangans mit schichtengitter. 2. Mangan (III)-manganat (IV). Helv. Chim. Acta 53, 453–464.

Gray, M.J., Malati, M.A., 1979. Adsorption from aqueous solution by d-manganese dioxide II. Adsorption of some heavy metal cations. J. Chem. Technol. Biotechnol. 29, 135–144.

Green-Pedersen, H., Jensen, B.T., Pind, N., 1997. Nickel adsorption on MnO_2, $Fe(OH)_3$, montmorillonite, humic acid and calcite: a comparative study. Environ. Technol. 18, 807–815.

Hayes, K.F., Redden, G., Ela, W., Leckie, J.O., 1991. Surface complexation models: an evaluation of model parameter estimation using FITEQL and oxide mineral titration data. J. Colloid Interface Sci. 142, 448–469.

Hedin, L., Lundqvist, S., 1969. Effects of electron–electron and electron–photon interactions on the one-electron states of solids. Solid State Phys. 23, 1–181.

Herbelin, A., Westall, J., 1996. A Computer Program for Determination of Chemical Equilibrium Constants from Experimental Data. Version 3.2. Department of Chemistry, Oregon State University, Corvallis, Oregon, p. 97331.

Jones, L.H.P., Milne, A.A., 1956. Birnessite, a new manganese oxide mineral from Aberdeenshire, Scotland. Mineral. Mag. 31, 283–288.

Kumar, R., Das, S.K., Ray, R.K., Biswas, A.K., 1994. A SEM backscattered electron mode study of microstructural features of ferromanganese nodules from central indian ocean basin. Trans. Indian Inst. Met. 47, 273–285.

Lanson, B., Drits, V.A., Silvester, E., Manceau, A., 2000. Structure of H-exchanged hexagonal birnessite and its mechanism of formation from Na-rich monoclinic buserite at low pH. Am. Mineral. 85, 826–838.

Lanson, B., Drits, V.A., Gaillot, A.-C., Silvester, E., Plancon, A., Manceau, A., 2002. Structure of heavy-metal sorbed birnessite: Part 1. Results from X-ray diffraction. Am. Mineral. 87, 1631–1645.

Larsen, F., Postma, D., 1997. Nickel mobilization in a groundwater well field: release by pyrite oxidation and desorption from manganese oxides. Environ. Sci. Technol. 31, 2589–2595.

Liu, L., Feng, Q., Yanagisawa, K., Bignall, G., Hashida, T., 2002. Lithiation reactions of Zn- and Li-birnessites in non-aqueous solutions and their stabilities. J. Mater. Sci. 37, 1315–1320.

Lumsdon, D.G., Evans, L.J., 1994. Surface complexation model parameters for goethite (α-FeOOH). J. Colloid Interface Sci. 164, 119–125.

Manceau, A., Gorshkov, A.I., Drits, V.A., 1992. Structural chemistry of Mn, Fe, Co, and Ni in manganese hydrous oxides: Part II. Information from EXAFS spectroscopy and electron and X-ray diffraction. Am. Mineral. 77, 1144–1157.

Manceau, A., Lanson, B., Drits, V.A., 2002a. Structure of heavy metal sorbed birnessite: Part III. Results from powder and polarized extended X-ray absorption fine structure spectroscopy. Geochim. Cosmochim. Acta 66, 2639–2663.

Manceau, A., Tamura, N., Marcu, M.A., MacDowell, A.A., Celestre, R.S., Sublett, R.E., et al., 2002b. Deciphering Ni sequestration in soil ferromanganese nodules by combining X-ray fluorescence, absorption and diffraction at micrometer scales of resolution. Am. Mineral. 87, 1494–1499.

McKenzie, R.M., 1980. The adsorption of lead and other heavy metals on oxides of manganese and iron. Aust. J. Soil Res. 18, 61–75.

McKenzie, R.M., 1989. Manganese oxides and hydroxides. In: Dixon, J.B., Weed, S.B. (Eds.), Minerals in Soil Environments. Soil Science Society of America, Madison, Wisconsin, pp. 493–502.

Murray, J.W., 1975. The interaction of metal ions at the manganese dioxide-solution interface. Geochim. Cosmochim. Acta 39, 505–519.

Nordstrom, D.K., Plummer, L.N., Wigley, T.M.L., Wolery, T.J., Ball, J.W., Jenne, E.A., et al., 1979. A Comparison of Computerized Chemical Models for Equilibrium Calculations in Aqueous Systems. In: Jenne, E.A. (Ed.), Chemical Modeling in Aqueous Systems, Speciation, Sorption, Solubility, and Kinetics, Series 93. American Chemical Society, pp. 857–892.

Parkhurst, D.L., Appelo, C.A.J., 1999. User's Guide to PHREEQC (Version 2)—A Computer Program for Speciation, Batch-Reaction, One-Dimensional Transport, and Inverse Geochemical Calculations: U.S. Geological Survey Water-Resources Investigations Report 99-4259. 312 pp.

Peacock, C.L., Sherman, D.M., 2004a. Copper(II) sorption onto goethite, hematite and lepidocrocite: a surface complexation model based on ab initio molecular geometries and EXAFS spectroscopy. Geochim. Cosmochim. Acta 68, 2623–2637.

Peacock, C.L., Sherman, D.M., 2004b. Vanadium(V) adsorption onto goethite (α-FeOOH) at pH 1.5 to 12: a surface complexation model based on ab initio molecular geometries and EXAFS spectroscopy. Geochim. Cosmochim. Acta 68, 1723–1733.

Peacock, C.L., Sherman, D.M., in press. Crystal-chemistry of Ni(II) in marine ferromanganese deposits: structural incorporation of Ni by Hx-birnessite. Am. Mineral.

Post, J.E., 1992. Crystal structures of manganese oxide minerals. In: Skinner, H.C.W., Fitzpatrick, R.W. (Eds.), Biomineralization Processes: Iron, Manganese. Catena Supplement 21. Catena, Cremlingen-Destedt, Germany, pp. 51–73.

Pretorius, P.J., Linder, P.W., 2001. The adsorptive characteristics of δ-manganese dioxide: a collection of diffuse double layer constants for the adsorption of H^+, Cu^{2+}, Ni^{2+}, Cd^{2+} and Pb^{2+}. Appl. Geochem. 16, 1067–1082.

Silvester, E., Manceau, A., Drits, V.A., 1997. Structure of synthetic monoclinic Na-rich birnessite and hexagonal birnessite: II. Results from chemical studies and EXAFS spectroscopy. Am. Mineral. 82, 962–978.

Som, S.K., Joshi, R., 2002. Chemical weathering of serpentinite and Ni enrichment in Fe oxide at Sukinda Area, Jajpur District, Orissa, India. Econ. Geol. 97, 165–172.

Tonkin, J.W., Balistrieri, L.S., Murray, J.W., 2004. Modeling sorption of divalent metal cations on hydrous manganese oxide using the diffuse double layer model. Appl. Geochem. 19, 29–53.

Villalobos, M., Toner, B., Bargar, J., Sposito, G., 2003. Characterization of the manganese oxide produced by *Pseudomonas putida* strain MnB1. Geochim. Cosmochim. Acta 67, 2649–2662.

Westall, J.C., Hohl, H., 1980. A comparison of electrostatic models for the oxide/solution interface. Adv. Colloid Interface Sci. 12, 265–294.

Wolery, T.J., 1979. Calculation of Chemical Equilibrium Between Aqueous Solution and Minerals—The EQ3/6 Software Package: Lawrence Livermore National Laboratory Report UCRL-52658. Livermore, CA.